ELSEVIER

Polymer 42 (2001) 9143–9154

polymer

www.elsevier.com/locate/polymer

Reactively compatibilised polymer blends: a case study on PA6/EVA blend system

Arup R. Bhattacharyya, Anup K. Ghosh, Ashok Misra*

Centre for Polymer Science and Engineering, Indian Institute of Technology, New Delhi 110016, India

Received 2 March 2001; received in revised form 15 March 2001; accepted 15 March 2001

Abstract

Reactive compatibilisation of immiscible polymers is becoming increasingly important and a representative study with PA6/EVA system is the focus of this paper. Morphological studies and crystallization behaviour of uncompatibilised and compatibilised blends of PA6/EVA were studied as functions of dispersed phase concentration (EVA or EVA-*g*-MA) and maleic anhydride (MA) content. Impact properties of the compatibilised PA6/EVA blends were studied as a function of MA content at fixed dispersed phase concentration. SEM studies of cryogenically fractured surfaces showed an increase in average domain size with increase in EVA level. On contrary, the average domain size and the domain size distributions reduced significantly in the presence of EVA-*g*-MA. This observation is found consistent with increase in EVA-*g*-MA concentration at a fixed MA level and also at a fixed concentration of dispersed phase with different level of MA in binary and ternary compositions. Morphological observations also revealed that the phenomenon of coalescence is slower in the presence of EVA-*g*-MA indicating the formation of in situ graft co-polymer at the interface. Impact strength of the compatibilised PA6/EVA blends increased significantly as compared to uncompatibilised PA6/EVA blends. Crystallization studies indicate that PA6 and EVA (or EVA-*g*-MA) crystallize separately at their bulk crystallization temperature. The degree of crystallinity is reduced marginally with increase in EVA level, whereas, the decrease in crystallinity is more in the presence of EVA-*g*-MA. SAXS studies indicate the superposition of PA6 and EVA lamellar scattering and the possible mode of insertion is random in nature. In case of reactive systems, SAXS studies also revealed the hindered crystal growth of PA6 and EVA due to the interfacial reaction.

Keywords: Reactive compatibilisation; Phase morphology; Crystallization behaviour

1. Introduction

The development of new multiphase polymeric materials with desired mechanical properties often involves the strategy of blending. A majority of polymer blends are thermodynamically immiscible in nature due to the low entropy of mixing [1]. The unfavourable entropy of mixing leads to the coarse and unstable phase morphology in binary blends with high interfacial tension and low interfacial adhesion [2]. Thus the mechanical properties of immiscible polymer blends are inherently inferior in nature. The problem of interfacial properties can be attenuated by introducing block or graft co-polymers, which in turn stabilise the phase morphology [3–5]. However, this strategy cannot be applied to all kinds of blends, and moreover, the synthesis of block or graft co-polymer is often very expensive. In recent times, much attention has been focussed to reactive compatibilisation. The reactive compatibilisation is based on the in situ formation of a block or graft co-polymers at the interface during melt blending [6]. This technique is very often used to stabilise the morphology of the immiscible polymer blends to obtain appropriate mechanical properties. It has also been reported that the modification of the interface by reactive method gives rise to finer and stable dispersion of domains as a result of suppression of coalescence [7]. Several studies have reported that the reactively compatibilised blends are characterized by a broad as well as less mobile interface, low interfacial tension and smaller domain size [8–10]. Groeninckx and co-workers studied the different aspects of reactive compatibilisation, e.g. the stabilisation of phase morphology, characterization of in situ formed graft co-polymer, width and location of phase co-continuity and the interfacial thickness in PA6 based blends [10–14]. It is reported that in situ formed graft co-polymer plays a crucial role in preventing the rate of

* Corresponding author. Address: Director, Indian Institute of Technology Bombay, Mumbai 400076, India. Tel.: +91-22-576-7001; fax: +91-22-572-3546.

E-mail address: amisra@cc.iitb.ernet.in (A. Misra).

0032-3861/01/$ - see front matter
PII: S0032-3861(01)00390-1

Table 1
Morphological parameters of PA6/EVA, PA6/EVA-*g*-MA and PA6/EVA/EVA-*g*-MA blends

Sample code	Blend composition, PA6/EVA/EVA-*g*-MA (wt%)	D_n (μm)	D_v (μm)	A_i ($\mu m^2/\mu m^3$)
N5	95/5/0	1.24	2.38	0.14
N10	90/10/0	1.43	2.69	0.24
N20	80/20/0	1.80	3.81	0.38
N30	70/30/0	2.70	14.31	0.38
NG5[a]	95/0/5 (MA = 1%)	0.17	0.36	35.3
NG10[a]	90/0/10 (MA = 1%)	0.19	0.33	31.5
NG20[a]	80/0/20 (MA = 1%)	0.29	0.59	20.7
NG30[a]	70/0/30 (MA = 1%)	0.38	0.65	15.8
NG20A	80/0/20 (MA = 1%)	0.44	1.21	3.89
NG20B	80/0/20 (MA = 2%)	0.29	0.59	6.66
NG20C	80/0/20 (MA = 4%)	0.12	0.05	25.0
NG20D	80/0/20 (MA = 6%)	0.09	0.22	30.0
NE10G10	80/10/10 (MA = 2%)	0.65	1.47	3.48
NE5G15	80/5/15 (MA = 2%)	0.34	0.52	7.31

[a] EVA-*g*-MA was procured commercially from Pluss Polymers, New Delhi, India.

coalescence. The interfacial thickness in reactive polymer blends is found to be thicker as compared to uncompatibilised blend [12]. The development of phase morphology in immiscible polymer blends has been investigated in detail by Macosko and co-workers [15]. It is reported that in the presence of reactive functional groups, the rate of coalescence is reduced drastically resulting in stable and finer domain size of the blends. They also investigated the role of interface in stabilization of morphology. Inoue and co-workers investigated the role of graft or block co-polymer at the interface in the reactively compatibilised blends [16–18]. The crystallization behaviour of uncompatibilised and compatibilised polymer blends is widely reported in the literature [19–22]. In case of uncompatibilised binary blends, the crystallization behaviour of one component is influenced by the presence of the other, which is reflected in the rate of crystallization, semi-crystalline morphology and the degree of crystallinity. However, in the case of reactively compatibilised blends, concurrent and fractionated crystallization of one of the components were found to take place in some of the systems. It is also reported that the rate of crystallization and semi-crystalline morphology are influenced in the reactively compatibilised blends. The effect of reactive compatibilisation on morphology, mechanical properties and crystallization behaviour was demonstrated successfully in PP/PBT and PA6/EVA system by Jain [23] and Bhattacharyya [24].

In the present paper, the effects of reactive compatibilisation using ethylene vinyl acetate grafted with maleic anhydride (EVA-*g*-MA) on phase morphology, impact properties and crystallization behaviour of compatibilised PA6/EVA blends are reported and compared with the uncompatibilised PA6/EVA blends.

2. Experimental

2.1. Materials

Polyamide6 (PA6) was obtained from Gujrat State Fertilizer, Vadodara, India (GUJLON M28RC, relative viscosity 2.8). Ethylene vinyl acetate (EVA) with vinyl acetate content 18% and MFI 2 gm/10 min (EVA 1802) from National Organic Chemical Industries, Mumbai, India was used as blending polymer. The ethylene vinyl acetate grafted with maleic anhydride (EVA-*g*-MA) was prepared in co-rotating, intermeshing twin screw extruder (ZSK25) using the temperature profile of 150–160°C at 150 rpm by varying the level of MA (1–6%) in presence of styrene and benzoyl peroxide. Commercial grade of ethylene vinyl acetate grafted with maleic anhydride (EVA-*g*-MA, Optim EVA 1802) with MA content of 1% was obtained from Pluss Polymer, New Delhi, India.

2.2. Blending and preparation of test specimens

The granules were dry-mixed in appropriate ratios and binary and ternary blends of PA6, EVA and EVA-*g*-MA were prepared in the co-rotating, intermeshing twin screw extruder (ZSK25, $L/D = 25$) with a screw speed of 150 rpm and 230°C. The detailed blending compositions are given in Table 1. The extruded strands were quenched immediately after extrusion in a water bath kept at room temperature. The extrudate were then chopped into granules and finally dried at 80°C for over 24 h before moulding. The component polymers were also extruded in the same way so that they would have the same thermal history as the blend compositions. Test specimens for determining the mechanical properties were prepared by injection moulding at 230°C and at screw speed of 80 rpm (Windsor SP-1).

2.3. Characterization studies

2.3.1. Morphology

Morphological studies were conducted by SEM analysis using a Cambridge Stereoscan Microscope (Model S4-10). For morphological analysis, cryogenically fractured tensile specimens were etched using *o*-xylene to remove EVA (or EVA-*g*-MA). For each blend, different micrographs were made and were analysed by image analyser to determine average domain size. Number average diameter (D_n) and volume average diameter (D_v) were determined according to the following relationships:

$$D_n = \frac{\sum N_i D_i}{\sum N_i} \quad (1)$$

$$D_v = \frac{\sum N_i D_i^3}{\sum N_i D_i^2} \quad (2)$$

where N_i and D_i are the number and the diameter of the ith domain, respectively. The interfacial area (A_{3D}) per unit

volume of dispersed phase (V_{3D}) was calculated from the total perimeter of the particles (P_{2D}) divided by the total area of the particles (A_{2D}) as obtained from the micrographs:

$$A_i\ (\mu m^2/\mu m^3) = \frac{P_{2D}}{A_{2D}} = \frac{A_{3D}}{V_{3D}} \quad (3)$$

2.3.2. Impact properties

Notched izod impact strength was measured on CEAST impact tester (Model Resil 25) following ASTM D-256. Impact strength measurements were made at 23°C. The test results reported are the average values of at least five specimens tested in each case to get a reliable value and the deviation of the data around the mean value was less than 5%.

2.3.3. Differential scanning calorimetry

Differential scanning calorimetry (DSC) measurements were carried out for all the blends and the pure polymers using Perkin Elmer DSC 7. The extruded samples of about 5 mg were dried in a vacuum oven prior to experiment. Thermograms were recorded during both heating and cooling cycle at 10°C/min using identical setting of instrument for all the samples. All the samples were first run through a heating cycle from 50 to 250°C and then through a cooling cycle after holding for 2 min at 250°C, to destroy any previous thermal history and crystallization. The degree of crystallinity (X_c) of PA6 phase was determined from the ratio of heat of fusion (ΔH_m) to the heat of fusion of 100% crystalline PA6, $(\Delta H_m)_0$, which was taken as 204.8 J/g [25]. The value of ΔH_m was normalized for the level of PA6 in the blend.

The heating scans were analysed to determine the melting behaviour of the components in the blends, such as the onset of melting (T_1), the melting peak temperature (T_2), completion of melting (T_4), the melting temperature range (T_4–T_1) and the heat of fusion (ΔH_m). Similarly, the cooling scans were used to determine the crystallization behaviour of the components of the blends, such as onset of crystallization (T_5), peak temperature of crystallization (T_6), completion of crystallization (T_7), width of crystallization exotherm (T_5–T_7) and heat of crystallization (ΔH_c).

2.3.4. Small angle X-ray scattering

Small angle X-ray scattering (SAXS) measurements at room temperature were carried out on a Rigaku Rotaflex, with rotating anode, and equipped with a Kratky camera. The data were recorded using a one-dimensional position sensitive proportional counter and an irradiation time of the samples of 30 min. Samples of 1 mm thickness were used for this study. The Lorentz corrected long period, L_w, was obtained from the maxima of $I(s)s^2$ versus s curves using Bragg's relationship,

$$L_w = \frac{1}{s} \quad (4)$$

The crystalline lamella thickness (L_c) was measured using the following relationship:

$$L_c = X_c L_w \quad (5)$$

where X_c is the volume crystallinity and is assumed to be equal to linear crystallinity. The long period L_w, is defined as the sum of the average thickness of the crystalline lamella thickness (L_c) and amorphous interlayer (L_a).

$$L_w = L_c + L_a \quad (6)$$

3. Results and discussion

3.1. Phase morphological analysis: PA6/EVA versus PA6/EVA-g-MA blends

This section deals with the morphological studies carried out using SEM for the PA6/EVA and PA6/EVA-*g*-MA binary blend systems with EVA or EVA-*g*-MA level varying from 0 to 50 wt%. The scanning electron micrographs of the PA6/EVA and PA6/EVA-*g*-MA blends are presented in Figs. 1 and 2, respectively. The micrographs show two different types of morphology dependent on the blend compositions. A particle-dispersed morphology was observed at EVA or EVA-*g*-MA level of 5–30 wt% (Figs. 1a–d and 2a–d), whereas, a co-continuous morphology was observed at 50 wt% EVA or EVA-*g*-MA (Figs. 1e and 2e). The morphological parameters in terms of the number average domain size (D_n), volume average domain size (D_v), interfacial area per unit volume of dispersed phase (A_i) obtained from the SEM analysis are presented in Table 1. The EVA domain size distributions in the blends of PA6/EVA and PA6/EVA-*g*-MA at different levels of EVA and EVA-*g*-MA are presented in Figs. 3 and 4.

It was found that the number average domain size (D_n) increased in PA6/EVA blends with an increase in the level of EVA. The value of D_n increases from 1.24 μm at 5 wt% EVA level to 2.70 μm at 30 wt% level of EVA. The domain size of the 50/50 combination of PA6/EVA-*g*-MA blend could not be measured due to its co-continuous nature. Fig. 3 depicts a significant increase in the width of the size distribution for the PA6/EVA blend; the largest size of the EVA domain varied from 4.6 to 22.2 μm as the EVA content in the blend changes from 5 to 30 wt%. This observation may be due to greater degree of coalescence in PA6/EVA blends with increase in EVA level. The detailed morphological analysis of PA6/EVA blends is reported separately [26].

The compatibilised PA6/EVA-*g*-MA blends, however, show a significant reduction in the domain size as compared to the uncompatibilised blends. The number average domain size in this case lies in the range of 0.17–0.38μm for an increase in EVA-*g*-MA level of 5–30 wt%. Furthermore, the domain size distribution increases with increase in the level of EVA-*g*-MA (Fig. 4). However, the distribution is

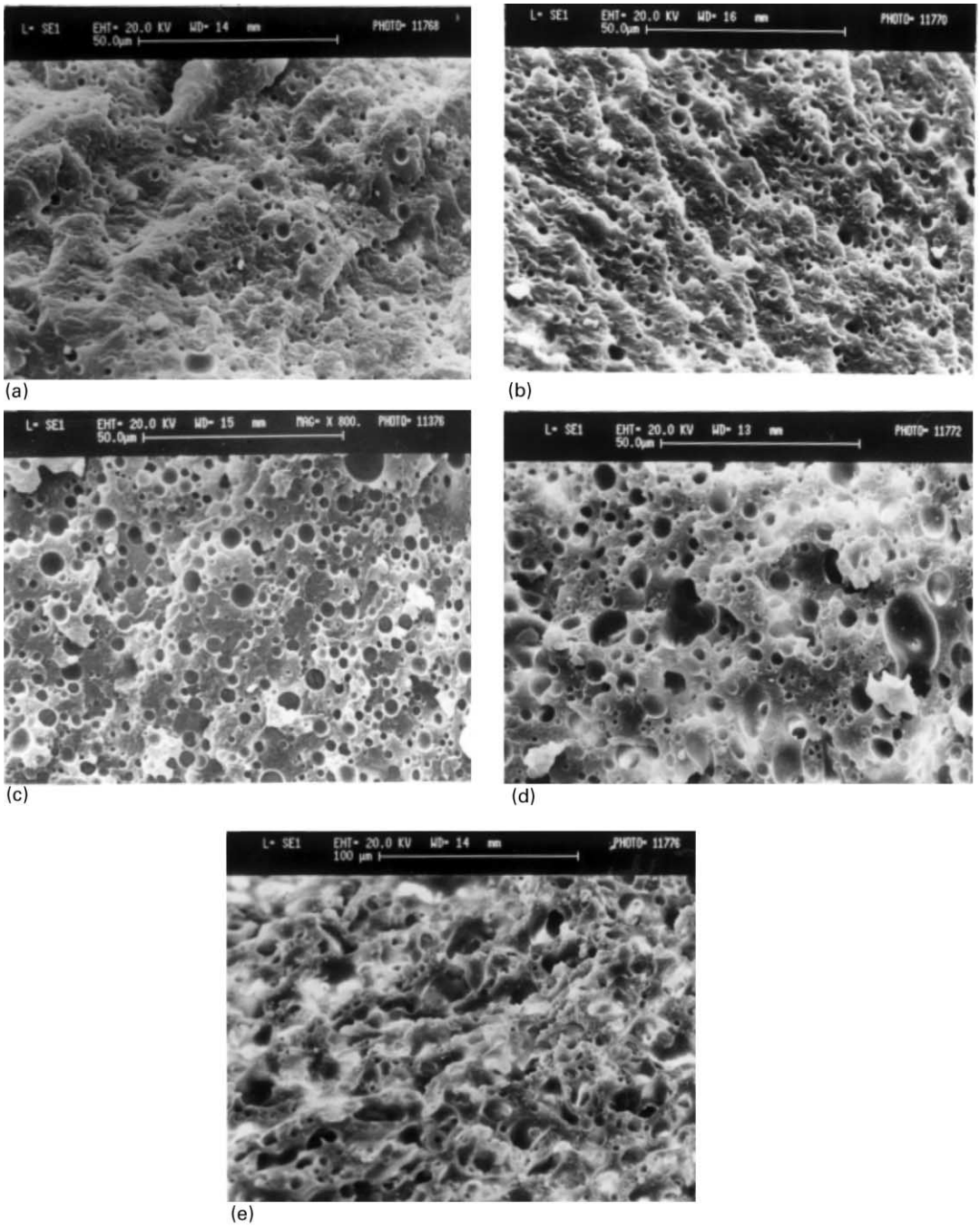

Fig. 1. Scanning electron micrographs of cryogenically fractured etched surfaces of PA6/EVA blends: (a) N5; (b) N10; (c) N20; (d) N30; (e) N50.

narrower in case of PA6/EVA-*g*-MA blends as compared to that of uncompatibilised PA6/EVA blends. This indicates that in presence of EVA-*g*-MA, the coalescence process is slower due to the in situ formation of graft co-polymer at the interface because of the reaction with anhydride functionality of MA and amine end group of PA6.

It has been reported that the interfacial area per unit volume of dispersed phase (A_i) is a measure of interfacial thickness in the multiphase polymer systems [13]. The values of A_i were found to increase marginally with the incorporation of EVA up to 20 wt% in the case of uncompatibilised blends (Table 1). On the other hand, the interfacial area per unit volume of dispersed phase was found to increase significantly in the case of PA6/EVA-*g*-MA blends.

In the case of PA6/EVA-*g*-MA blends, the formation of in situ graft co-polymer between amine end group of PA6 and anhydride functionality of MA prevent the rate of coalescence suggesting an emulsifying effect with finer dispersion via the faster size reduction process. Thus, the larger size domains in case of uncompatibilised blends get converted into smaller size domains with narrower size distribution in case

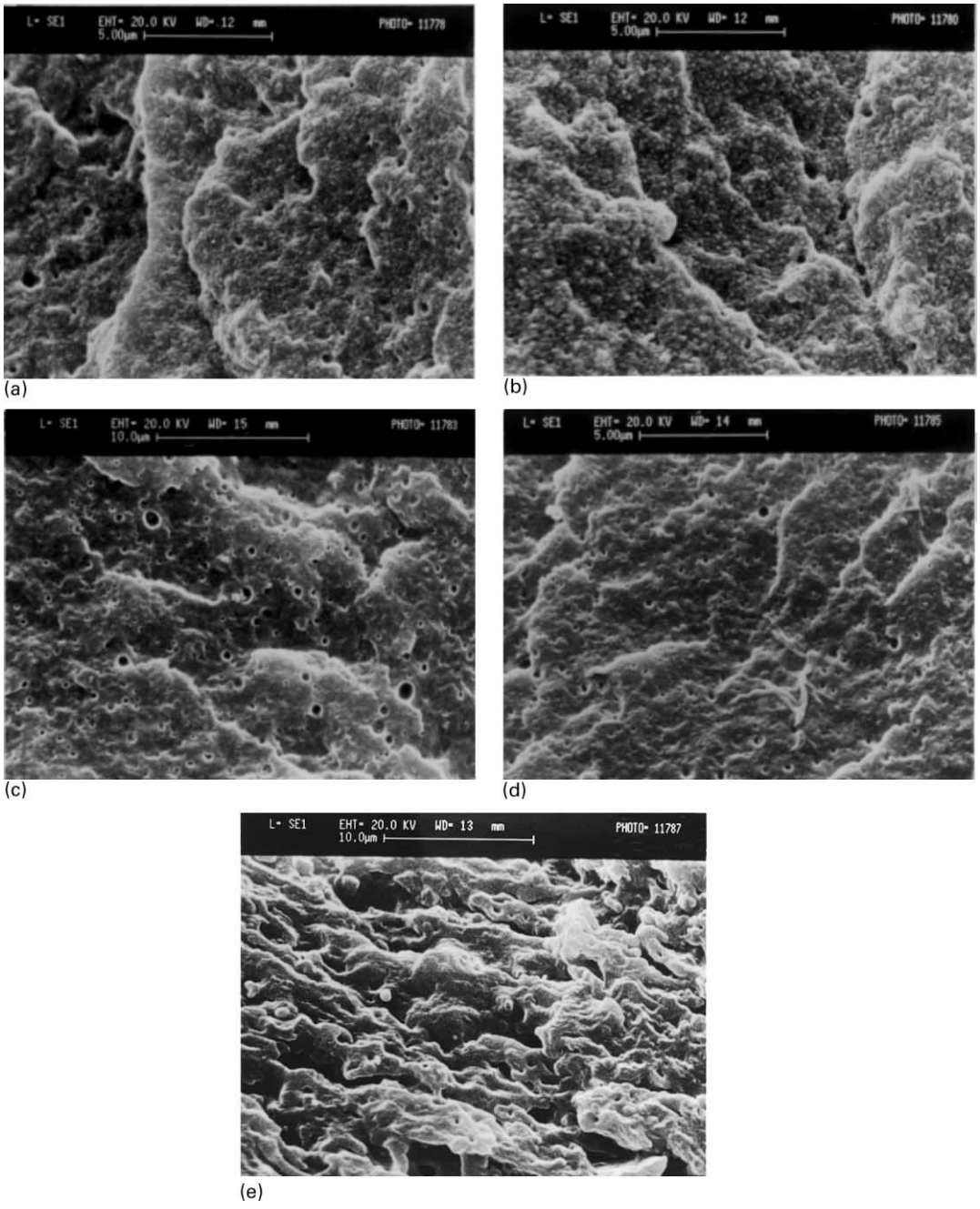

Fig. 2. Scanning electron micrographs of cryogenically fractured etched surfaces of PA6/EVA-*g*-MA blends: (a) NG5; (b) NG10; (c) NG20; (d) NG30; (e) NG50.

of compatibilised blends. It has been reported by Sundararaj and Macosko [15] that addition of di-block co-polymer in the uncompatibilised blend or use of functional polymer suppresses coalescence at higher concentrations of compatibiliser. In case of reactive blends, reaction is more efficient since it suppresses coalescence effects at concentration up to 30 wt%. In contrast, the 50/50 combination of PA6/EVA-*g*-MA blend shows the presence of co-continuous morphology. This phenomenon has also been observed by Thomas and Groeninckx [7]. They reported that the addition of compatibiliser, though reduced the particle size in the compatibilised PA6/EPM blends, did not have any influence on the location of phase continuity. They also observed a co-continuous morphology with 40–70 wt% EPM level at high concentration of the compatibiliser.

3.2. Effect of MA level on phase morphology of the compatibilised blends

The scanning electron micrographs of compatibilised

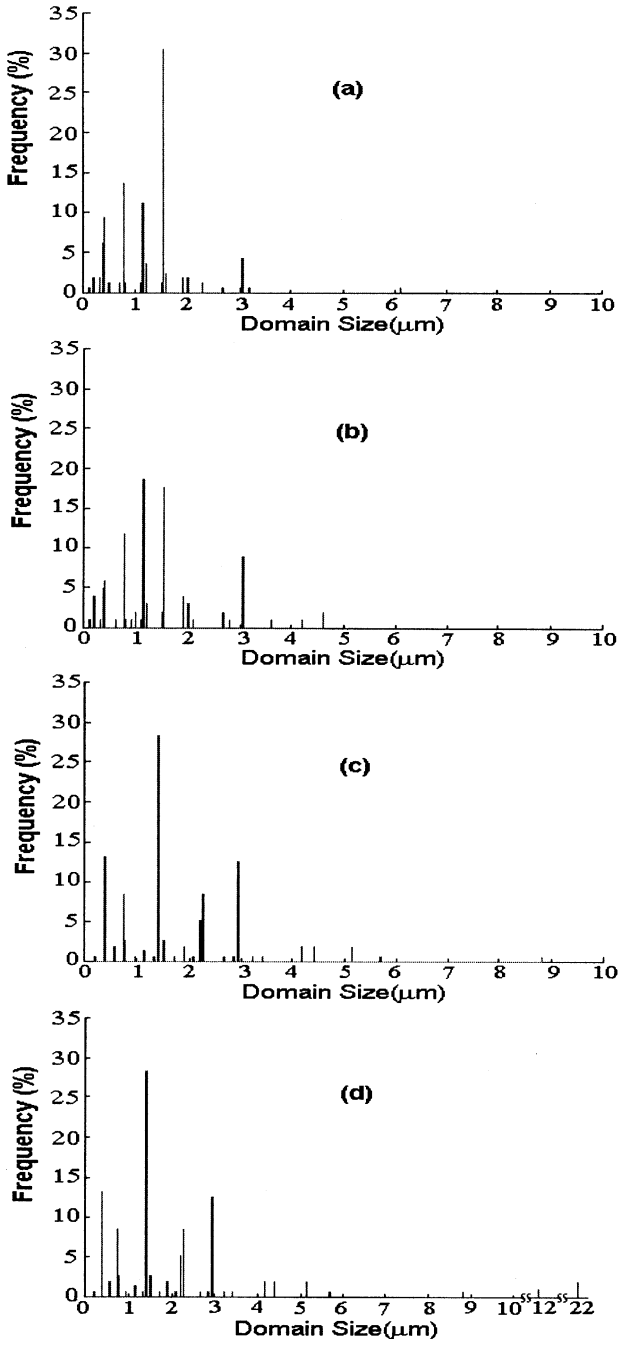

Fig. 3. Domain size distribution of PA6/EVA blends: (a) N5; (b) N10; (c) N20; (d) N30.

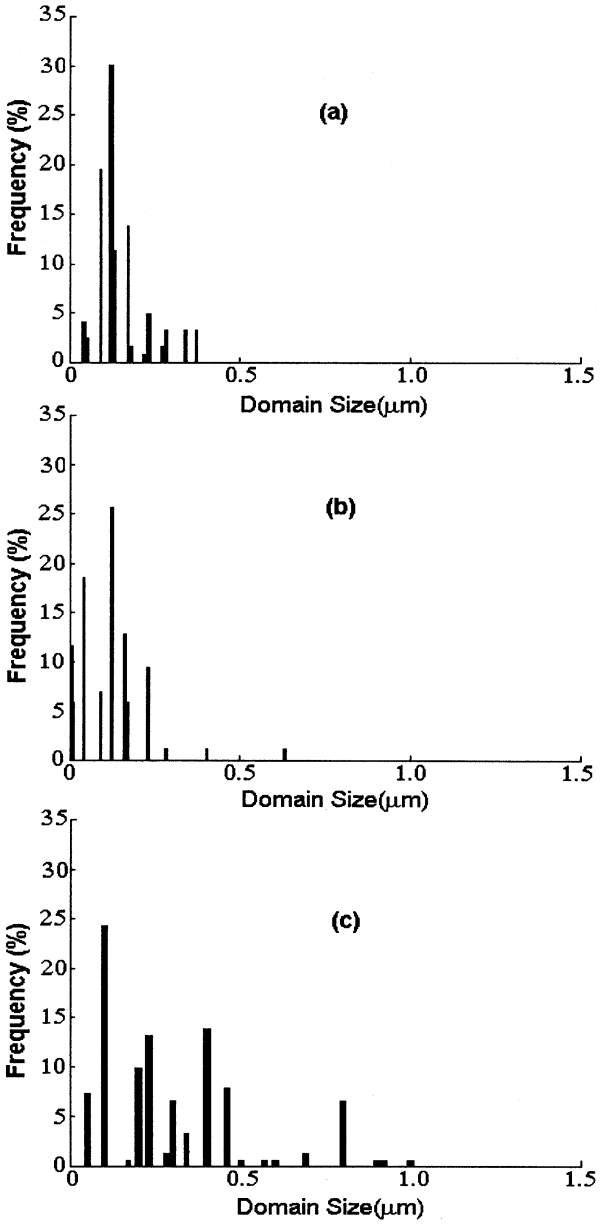

Fig. 4. Domain size distribution of PA6/EVA-*g*-MA blends: (a) NG5; (b) NG10; (c) NG20.

blends such as PA6/EVA-*g*-MA and PA6/EVA/EVA-*g*-MA are presented in Fig. 5. In all the compositions, the dispersed phase concentration was maintained at 20 wt%. A particle-dispersed type of morphology was observed for all these compositions. The morphological parameters (D_n, D_v, A_i) are presented in Table 1. The domain size distributions of EVA-*g*-MA of these blends are presented in Fig. 6. The SEM analysis indicates a very significant reduction in the domain size for all the compositions compared to that of the uncompatibilized 80/20 PA6/EVA blends (Table 1). The value of D_n reduced from 1.8 μm in the case of 80/20 PA6/EVA blend to 0.2 μm in PA6/EVA-*g*-MA blend (MA content of 4%). Systematic increase of MA level in EVA-*g*-MA decreases the average domain size of EVA-*g*-MA significantly. It is also evident from Table 1 that incorporation of higher amount of EVA-*g*-MA in the ternary blends of PA6/EVA/EVA-*g*-MA reduces the average domain size considerably. This may be due to the higher amount graft co-polymer formation between amine end group of PA6 and anhydride functionality of MA in the interface of PA6 and EVA.

The interfacial area per unit volume of dispersed phase, A_i increases significantly with higher level of MA in PA6/EVA-*g*-MA blends. This trend is found similar with higher

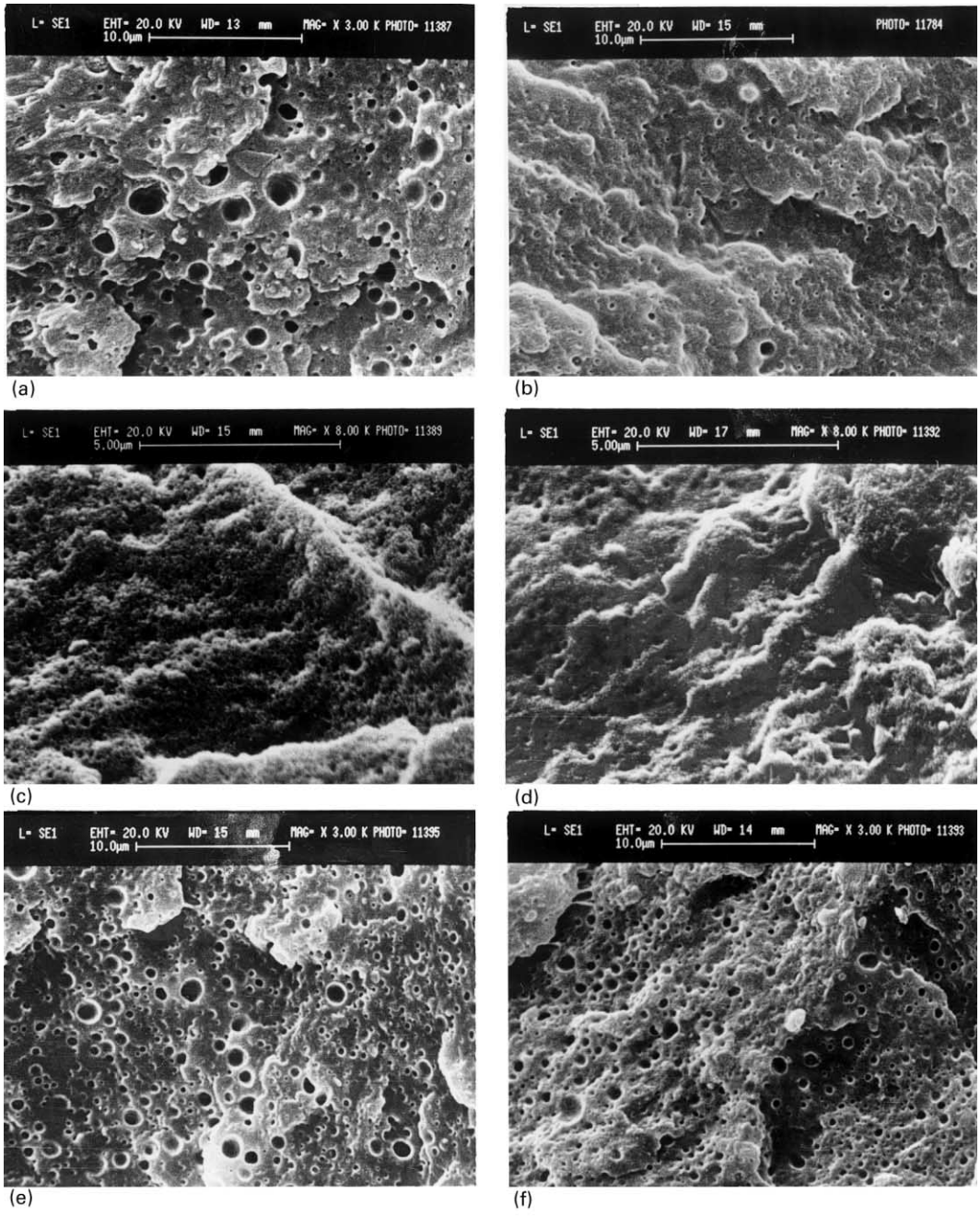

Fig. 5. Scanning electron micrographs of cryogenically fractured etched surfaces of PA6/EVA-*g*-MA and PA6/EVA/EVA-*g*-MA blends: (a) NG20A; (b) NG20B; (c) NG20C; (d) NG20D; (e) NE10G10; (f) NE5G15.

amount of EVA-*g*-MA level in the ternary blends of PA6/EVA/EVA-*g*-MA. The increase in interfacial area in reactively compatibilised blends may be due to formation of diffuse interphase. In contrast, uncompatibilised PA6/EVA blends are characterised by sharp interphase.

In brief, the reactively compatibilised blends are characterized by small domain size with narrow domain size distribution, higher interfacial thickness and immobile interface in contrast to large domain size and distribution, sharp and mobile interface in the case of uncompatibilised blends.

3.3. Impact properties

EVA co-polymer was found to increase the notched impact strength in general, however, the extent of impact modification is minimal due to its immiscibility/incompatibility with PA6 [26]. The plot of notched izod impact strength for PA6/EVA binary blends as a function of EVA wt% is presented in Fig. 7. At 23°C, the notched impact strength of PA6 increased at all levels of EVA, the value being 1.2–2.1 times that of pure PA6 depending on the blend composition. Hence, effort has been made to enhance

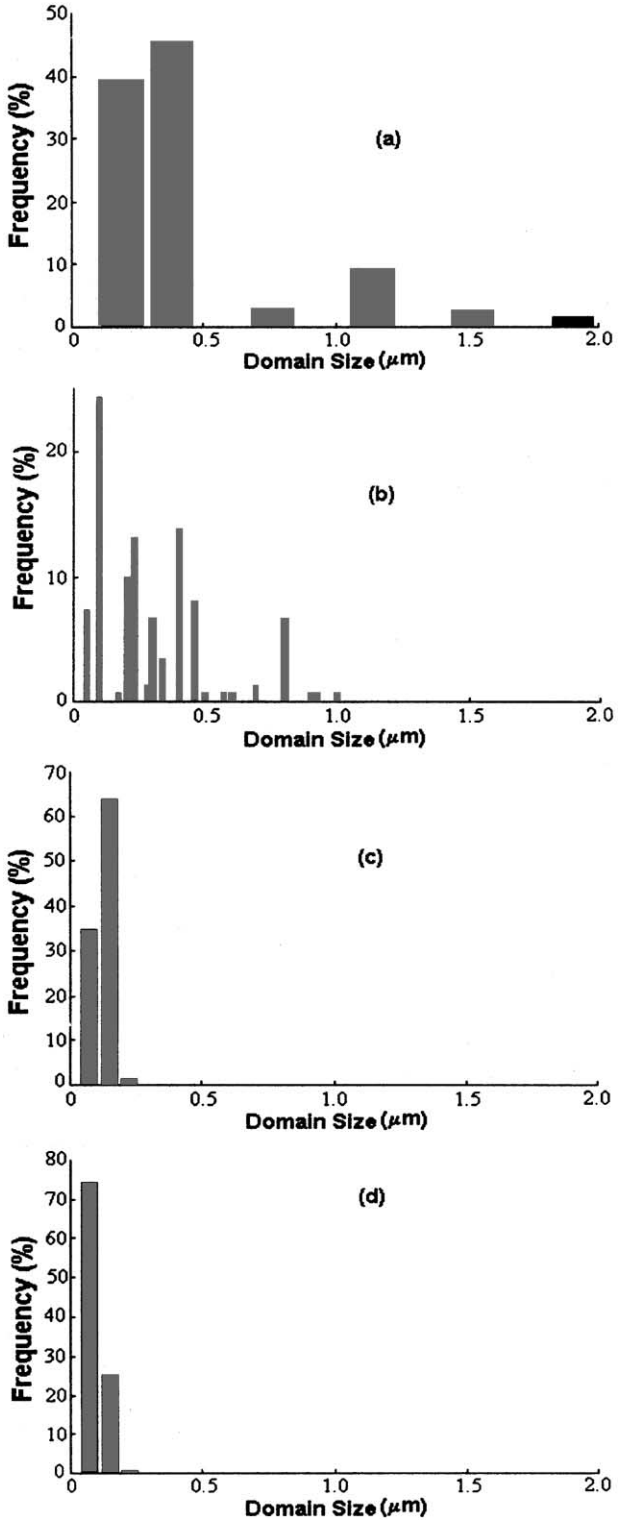

Fig. 6. Domain size distribution of PA6/EVA-*g*-MA blends: (a) NG20A; (b) NG20B; (c) NG20C; (d) NG20D.

the impact strength of PA6/EVA blends by introducing EVA-*g*-MA. The plot of notched impact strength for PA6/EVA-*g*-MA binary blends as function of MA levels is presented in Fig. 8. The notched impact strength of PA6

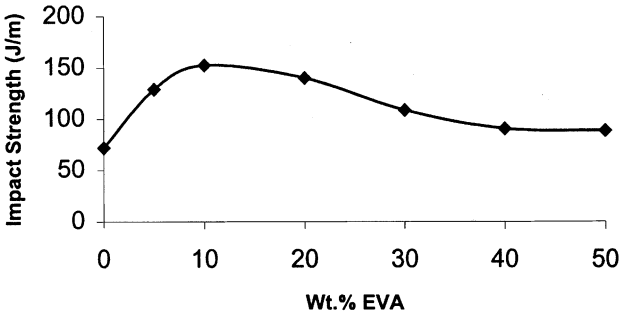

Fig. 7. Impact strength versus EVA content (wt%) in PA6/EVA blends.

increased marginally on incorporation of 20 wt% EVA, the increase in impact strength is about two times as compared to pure PA6. On the other hand, the notched impact strength of the PA6/EVA-*g*-MA blends increased significantly as compared to 80/20 PA6/EVA blends. It is evident from the plot (Fig. 8) that at 23°C, the notched impact strength increased at all levels of EVA-*g*-MA, the value being 3.5–6.2 times that of 80/20 PA6/EVA depending on the MA level. The maximum impact strength was achieved at 6 wt% MA level at this test temperature. The plot of impact strength for PA6/EVA/EVA-*g*-MA blends as a function of EVA-*g*-MA level at fixed MA level (2%) is presented in Fig. 9. It is observed from the plot that the impact strength increased at all levels of EVA-*g*-MA, the value being 4.2–4.7 times as compared to that of 80/20 combination of PA6/EVA depending on the EVA-*g*-MA level. In general, all the compositions showed tough behaviour at 23°C and the entire fracture surface stress whitened under impact failure. The higher impact strength of these systems is presumably due to better interfacial adhesion between PA6 and EVA, thus promoting better stress transfer. It has also been reported that amine end group of PA6 and anhydride functionality of MA react to form graft copolymer at the interface [27]. The increase in impact strength in PA6/EVA-*g*-MA and PA6/EVA/EVA-*g*-MA blends with increase in MA level may be due to enhanced extent of reaction between the amine end group and the anhydride functionality of MA.

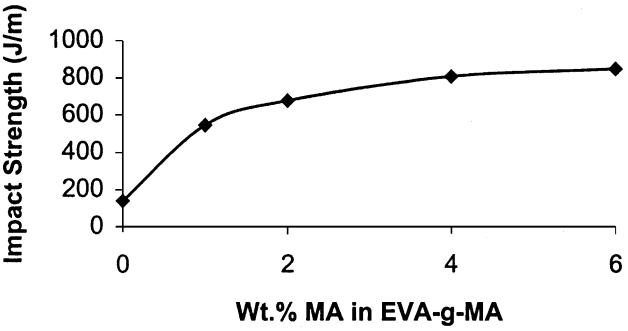

Fig. 8. Impact strength versus MA level (wt%) in PA6/EVA-*g*-MA blends.

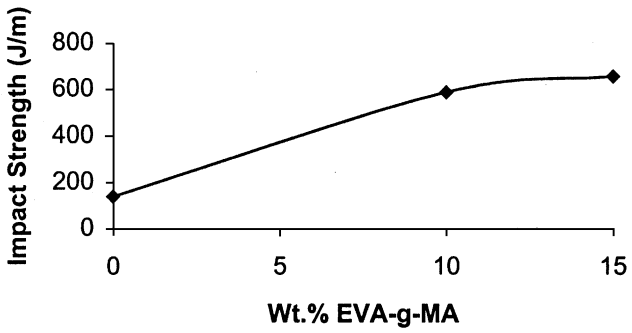

Fig. 9. Impact strength versus EVA-*g*-MA (MA = 2%) content in PA6/EVA/EVA-*g*-MA blends.

3.4. Crystallization studies: PA6/EVA versus PA6/EVA-g-MA blends

3.4.1. DSC analysis

The DSC melting endotherms and crystallization exotherms of PA6/EVA and PA6/EVA-*g*-MA blends together with those of pure components are presented in Figs. 10 and 11. The thermal data has been summarised in Table 2. The melting endotherm of pure PA6 and EVA showed the presence of one peak in the DSC heating scan (Fig. 10). The melting peak temperature for pure PA6 is 226.8°C whereas that of pure EVA corresponds to 92°C. The melting endotherms of PA6/EVA blends showed two melting peaks, one corresponding to PA6 and the other to EVA. The melting peak temperature (T_m) of PA6 showed a depression in melting point by 4–5°C depending on the blending ratio indicating some miscibility of the amorphous phase in the melt. The onset of melting of PA6 decreases significantly on incorporation of EVA. The increase in melting peak width continues up to 30 wt% EVA; the values then decrease with further increase in EVA content. This suggests that on incorporation of EVA up to 30 wt%, the crystal size of PA6 gets smaller while the crystal size distribution gets broader. Beyond 30 wt% EVA content, the PA6 crystals get smaller with narrower crystal size distribution. The percent crystallinity, calculated from the melting endotherm, of PA6 component was found to be almost constant in the entire composition range, showing a decrease of 4% at 50 wt% EVA level, being within experimental error. Similarly, crystallization exotherms (Fig. 11) of the PA6/EVA blends, when cooling from the melt, showed two exothermic peaks, one corresponding to PA6 (around 189°C) and the other corresponding to EVA (around 71°C). In brief, the two components are crystallizing separately, however, the crystallization behaviour of one component is being affected by the presence of other phase. A similar analysis has been reported for PBT/HDPE blends [28].

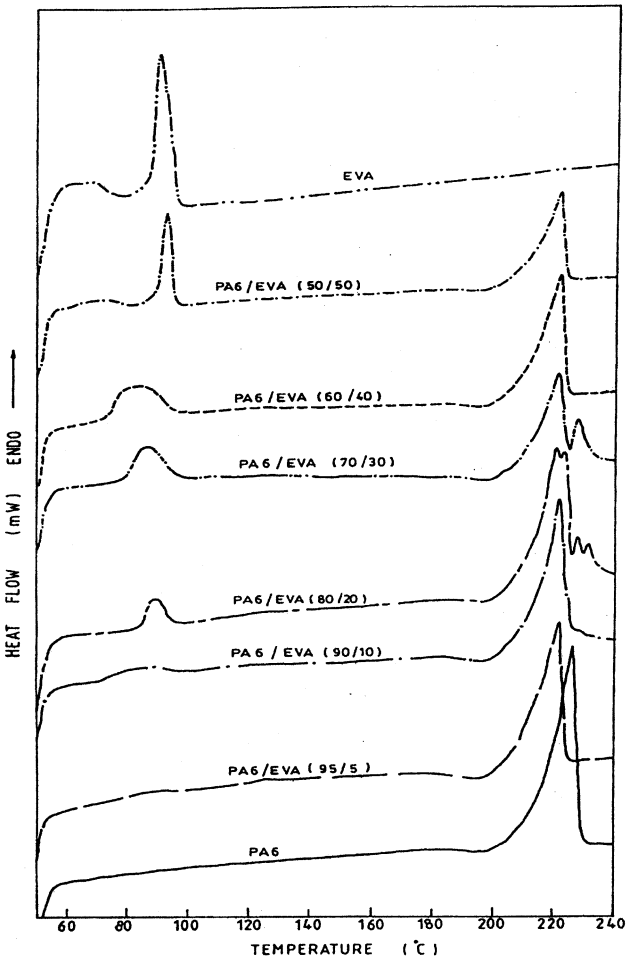

Fig. 10. DSC melting endotherms of PA6/EVA blends.

All the blend compositions of PA6/EVA-*g*-MA have been found to exhibit two melting endotherms, one corresponding to PA6 component and the other corresponds to EVA-*g*-MA. An analysis of the melting endotherms (Table 2) revealed that on addition of EVA-*g*-MA, there is a depression in peak temperature of the PA6 phase by 4–5°C accompanied by a decrease in the percent crystallinity of the PA6 phase. The degree of crystallinity was found to decrease from 34% in pure PA6 to 28.4% in 50/50 combination of PA6/EVA-*g*-MA blend. The depression of the peak temperatures may be accounted as part of the amorphous phase migrates to other phase, thus rendering some miscibility between PA6 and EVA-*g*-MA in the melt state. It was also found from the analysis that the onset of melting of PA6 decreased with broader peak width, which indicates the formation of smaller PA6 crystal with broader crystal size distribution.

The DSC cooling scans were used to determine the crystallization behaviour of the two components in the blends. It is observed from the crystallization exotherm that pure PA6 crystallizes at around 189.8°C, whereas, EVA-*g*-MA crystallizes at around 72°C. The analysis of the crystallization exotherms is presented in Table 2. It is evident from Table 2 that the heat of crystallization of PA6 decreased significantly, whereas, the onset of crystallization of PA6 phase and the crystallization peak temperature remained practically unchanged. The crystallization behaviour of the

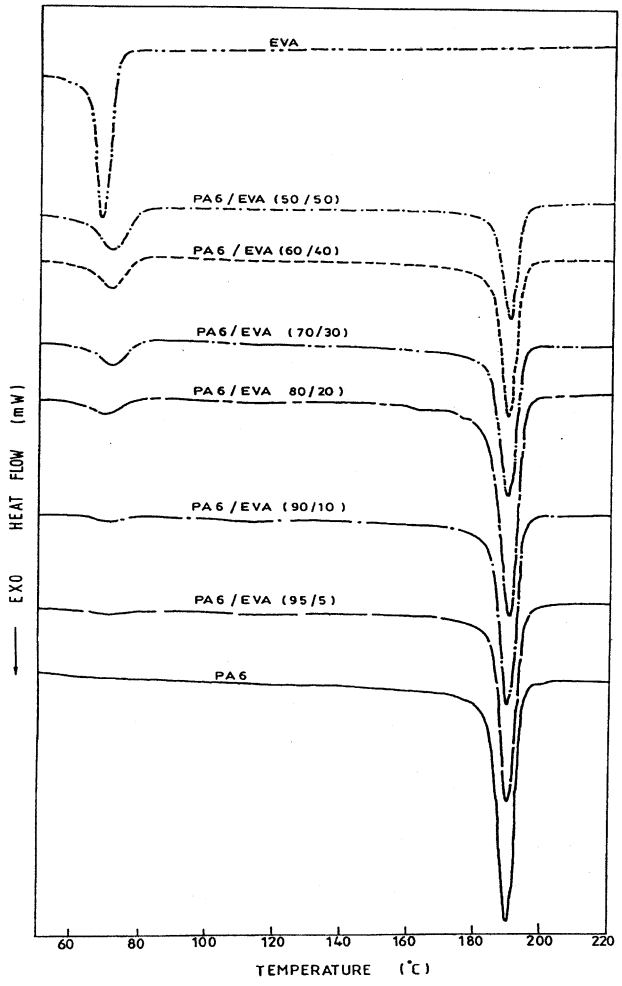

Fig. 11. DSC crystallization exotherms of PA6/EVA blends.

PA6/EVA-*g*-MA blends may be influenced by two factors: PA6 solid particles may be acting as a nucleating agent for EVA-*g*-MA phase and at the same time the reaction at the interface may hinder the rate of crystallization of both the components.

3.5. Effect of MA level in crystallization behaviour of compatibilised blends

3.5.1. DSC analysis

The melting parameters and the crystallization parameters are presented in Table 2. In these blends, the ratio of PA6 to EVA or combination of EVA and EVA-*g*-MA was maintained as 80/20 in all cases. It is evident from Table 2 that the PA6 phase of the reactively compatibilized blends is affected on addition of EVA-*g*-MA, indicating lower amount of crystallinity. The lowering of crystallinity of PA6 is more appreciable in case of ternary blends of PA6/EVA/EVA-*g*-MA as compared to PA6/EVA-*g*-MA blends.

It is evident from Table 2 that the onset of crystallization and the crystallization peak temperature of PA6 in these alloys showed no appreciable change indicating little change in the crystal structure of PA6. It is also to be noted that the only appreciable change was observed in the heat of crystallization of PA6 component. The lowering of heat of crystallization with higher MA content of EVA-*g*-MA suggests the formation of graft co-polymer between the amine end group of PA6 and anhydride functionality at the interface. This graft co-polymer, in turn, affects the mobility of PA6 chain, thus lowering the crystallization. This phenomenon was also observed by several researchers [21,22]. Similarly, the heat of crystallization of EVA-*g*-MA phase in all the ternary alloys was also lowered as compared to that of EVA phase of 80/20 PA6/EVA blend.

Table 2
Melting and crystallization parameters of PA6 in PA6/EVA, PA6/EVA-*g*-MA and PA6/EVA/EVA-*g*-MA blends

Sample code	Melting parameters				Crystallization parameters			
	Onset (T_1, °C)	Completion (T_4, °C)	Peak width (T_4–T_1)	X_c (%)	Onset (T_5, °C)	Completion (T_7, °C)	Peak width (T_5–T_7)	ΔH_c (J/g)
PA6	218.7	233.2	14.5	34.0	193.7	153.3	40.4	64.7
N5	211.1	227.0	15.9	30.5	194.1	151.0	43.1	60.2
N10	216.1	235.4	19.3	28.6	193.8	151.5	42.3	64.3
N20	211.9	235.4	23.5	29.1	193.7	152.0	41.7	62.4
N30	212.0	236.9	24.9	29.8	193.8	153.3	40.5	62.0
N50	213.6	227.3	13.7	30.3	193.5	168.4	25.1	57.2
NG5	211.9	230.6	18.7	31.4	192.6	159.3	33.3	60.0
NG10	213.5	230.5	17.0	30.0	193.3	166.9	26.4	49.5
NG20	214.6	229.0	14.4	30.3	191.3	160.8	30.5	59.0
NG30	213.5	226.4	12.9	30.5	192.0	165.4	26.6	58.4
NG50	207.4	226.4	19	28.4	191.3	165.4	25.9	30.6
NG20A	212.9	233.2	20.3	29.0	193.5	159.4	159.4	34.1
NG20B	209.6	233.4	27.8	28.4	193.2	163.7	163.7	29.5
NG20C	206.7	228.7	22.0	23.5	192.1	162.4	162.4	29.7
NG20D	212.6	228.9	16.3	22.5	192.0	159.3	159.3	32.7
NE10G10	211.2	228.4	17.2	28.5	193.0	161.1	31.7	59.0
NE5G15	212.3	228.5	16.2	28.0	192.6	160.3	32.3	58.7

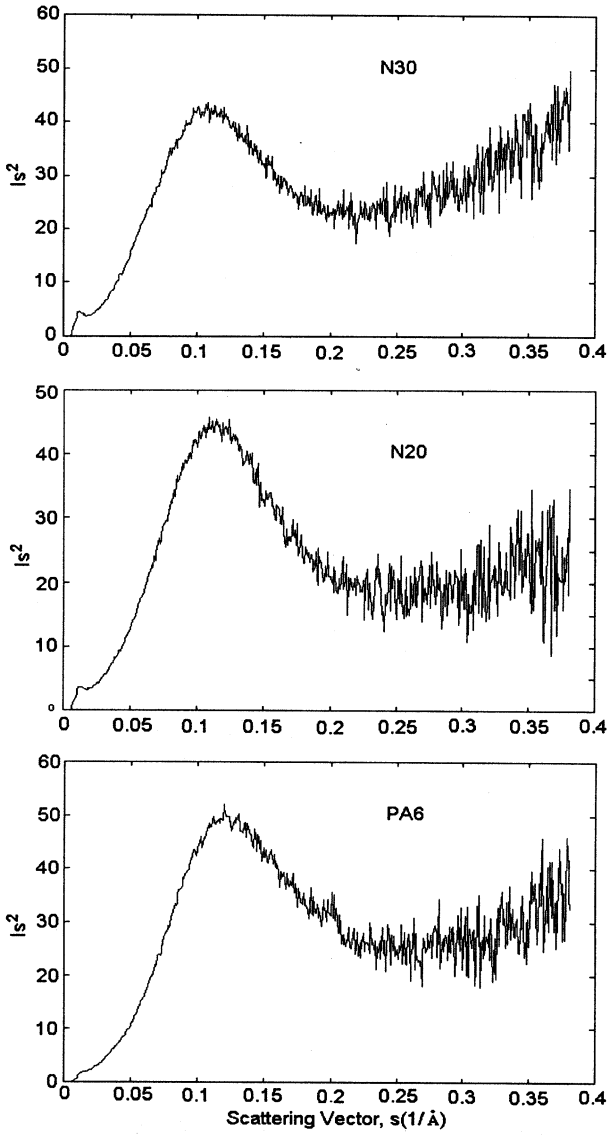

Fig. 12. Lorentz corrected SAXS profile of PA6 and PA6/EVA blends.

In brief, the reactively compatibilised PA6/EVA-*g*-MA and PA6/EVA/EVA-*g*-MA alloys are crystallizing separately at the bulk temperature of crystallization of their individual components accompanied by lower heat of crystallization.

3.6. Crystallization studies: PA6/EVA versus PA6/EVA-g-MA blends

3.6.1. SAXS analysis

The Lorentz corrected scattering profiles (Is^2 versus *s*-curve) of pure PA6 together with its blends obtained at room temperature are shown in Fig. 12. The plot for PA6 shows one peak as would be expected. The blends also show one peak, which is broader than that of PA6. It is believed that the peak for the blends arises from a superposition of contribution from the crystalline structure of PA6 and EVA resulting in its broadening over

Table 3
SAXS analysis of PA6, PA6/EVA, PA6/EVA-*g*-MA and PA6/EVA/EVA-*g*-MA blends

Sample	Long period, L_w (nm)	Crystalline lamella thickness, L_c (nm)	Amorphous thickness, L_a (nm)
PA6	80.0	41.6	38.4
N5	85.7	36.0	49.7
N10	87.8	38.6	49.1
N20	94.7	42.6	52.1
N30	94.7	22.7	72.0
N50	93.5	44.8	48.6
NG5	81.0	38.5	42.5
NG20	84.0	35.6	48.4
NG30	84.2	34.2	50.0
NG50	92.6	34.0	58.6
NG20A	92.3	45.1	47.2
NG20B	90.0	41.4	48.6
NG20D	88.8	31.7	57.1
NE10G10	87.8	34.4	53.3
NE5G15	87.8	38.5	49.3

PA6. The long period, crystalline lamella thickness and amorphous interlayer thickness of PA6 and its blends were calculated from scattering profile and reported in Table 3. It is observed from Table 3 that on addition of EVA, the long period of the PA6/EVA blends increased as compared to that of PA6. In these blends, there was a decrease in the crystalline lamella thickness and a corresponding increase in the amorphous interlayer thickness, at EVA level of 30 wt%. As suggested earlier the peak observed at room temperature is a superposition of PA6 and EVA lamellar scattering since both these components in the blends are semi-crystalline at temperatures below the melting point of EVA. The long periods measured from these samples represent an average size of the PA6 and EVA lamellae. This observation could suggest that the PA6 and EVA lamellae are randomly mixed, as a segregated arrangement will give rise to two peaks in the scattering profile [29–32]. Similarly, on incorporation of EVA-*g*-MA, the long period of the PA6/EVA-*g*-MA blends was found to increase as shown in Table 3, however, the increase is less as compared to PA6/EVA blends. The same explanation can be given to PA6/EVA-*g*-MA blends as well. PA6 and EVA-*g*-MA lamellae are randomly mixed in case of PA6/EVA-*g*-MA blends. Cheung and co-workers investigated the small angle scattering in poly(caprolactone)/polycarbonate blends and reported the same kind of observation at room temperature scattering profile [19].

3.7. Effect of MA level in crystallization behaviour of compatibilised blends

3.7.1. SAXS analysis

The data generated in the small angle X-ray scattering of the reactively compatibilised blends are presented in Table 3, which shows that the long spacing of these alloys is found to decrease considerably as compared to

that of uncompatibilised blend, but the value is higher than that of pure PA6. This again suggests that the long periods represent an average size of the PA6 and EVA-*g*-MA lamellae, which randomly mixed in the blends. On incorporation of higher level of MA in EVA-*g*-MA, the long period of the blends progressively decreased indicating higher amount of interfacial reaction between amine end group of PA6 and anhydride functionality of MA. The lower values of long period also suggest the hindered crystal growth of PA6 in presence of EVA-*g*-MA. This observation is in compliance with the lower overall crystallinity found in these compositions from DSC analysis.

4. Conclusions

Reactive compatibilisation has been effectively used to suitably modify the morphology and in turn enhance the impact strength. The blend system of PA6/EVA was taken as a representative case for the study. Similar approach is being employed for other immiscible polymer blend systems such as PBT/PP blends [23]. The major conclusions of the present study are as follows:

1. PA6 and EVA form incompatible blends as seen by morphological studies. The increase in average domain size in PA6/EVA blends indicates higher rate of coalescence with increase of EVA level.
2. In presence of EVA-*g*-MA, the coalescence process is reduced drastically due to the in situ formation of graft co-polymer at the interface.
3. The formation of finer and stable dispersion is also found with different level of MA content in PA6/EVA-*g*-MA blends.
4. The notched impact strength of the reactively compatibilised blends of PA6 and EVA is significantly higher as compared to that of uncompatibilised PA6/EVA blends.
5. PA6 and EVA crystallize separately at their bulk crystallization temperature. The same trend is found in PA6/EVA-*g*-MA blends. But, the degree of crystallinity of PA6 phase is affected strongly in reactively compatibilised blends.
6. SAXS analysis revealed an increase in long period in the blends of PA6/EVA and PA6/EVA-*g*-MA with increase in dispersed phase concentration; which may be arising due to the superposition of PA6 and EVA or EVA-*g*-MA lamellae. The possible insertion mode may be random in nature. The crystal growth of PA6 and EVA-*g*-MA was hindered with increase in MA content in EVA-*g*-MA as indicated from the decrease in long period compared to uncompatibilised PA6/EVA blends.

Overall, it can be concluded that EVA-*g*-MA is found to be an efficient compatibiliser in case of PA6/EVA blends. The effect of compatibilisation can be seen from the studies of phase morphology, impact property and crystallization behaviour.

Acknowledgements

The authors wish to acknowledge the help and support provided to one of the authors (ARB) by Prof. Gabriel Groeninckx for carrying out part of the work in the Laboratory of Macromolecular Structural Chemistry, Department of Chemistry, Katholieke University, Leuven, Belgium.

References

[1] Paul DR, Newman S. Polymer blends, vol. 1. New York: Academic Press, 1979.
[2] Utracki LA, Favis BD. Polymer alloys and blends. In: Cheremisinoff NP, editor. Encyclopedia of engineering materials. New Jersey: Marcel Dekker, 1988.
[3] Macosko CW, Guegan P, Khandpur AK, Nakayama A, Marechal P, Inoue T. Macromolecules 1996;29:5590.
[4] Sundararaj U, Macosko CW. Macromolecules 1995;28:2647.
[5] Teyssie P, Fyat R, Jerome R. Macromol Chem 1986;187:837.
[6] Inoue T. Paper presented at PPS15; 1999, The Netherlands.
[7] Thomas S, Groeninckx G. Polymer 1999;40:5799.
[8] Scott CE, Macosko CW. Polymer 1994;35:5422.
[9] Li H, Chiba T, Higashida N, Yang Y, Inoue T. Polymer 1997;38:3921.
[10] Dedecker K, Groeninckx G. Polymer 1998;39:4985.
[11] Dedecker K, Groeninckx G. Polymer 1998;39:4993.
[12] Dedecker K, Groeninckx G. Polymer 1998;39:5001.
[13] Dedecker K, Groeninckx G. Macromolecules 1999;32:2472.
[14] Dedecker K, Groeninckx G. J Appl Polym Sci 1999;73:889.
[15] Sundararaj U, Macosko CW. Macromolecules 1995;28:2647.
[16] Charoensirisomboon P, Chiba T, Torikai K, Saito H, Ougizawa T, Inoue T, Weber M. Polymer 1999;40:6975.
[17] Charoensirisomboon P, Chiba T, Inoue T, Weber M. Polymer 2000;41:5977.
[18] Okamoto M, Inoue T. Polym Engng Sci 1993;33:175.
[19] Cheung YW, Stein RS, Wignall GD, Yang HE. Macromolecules 1993;26:5365.
[20] Nadkarni VM, Jog JP. Crystallization of polymers in thermoplastic blends and alloys, Handbook of polymer science and engineering, vol. 4. New York: Marcel Dekker, 1989. p. 81.
[21] Ikkala OT, Holsti-Miettinen RM, Seppalla J. J Appl Polym Sci 1993;49:1165.
[22] Moon HS, Ryoo BK, Park JK. J Polym Sci, Polym Phys 1994;32:1427.
[23] Jain P. Studies on reactive blending and structure development of PP based blends. PhD Thesis. India: IIT Delhi; 2001.
[24] Bhattacharyya AR. Structure property relationship studies on PA6/EVA blends and alloys. PhD Thesis. India: IIT Delhi; 2000.
[25] Brandrup J, Immergut EH. Polymer hand book. 2nd ed. New York: Wiley, 1975.
[26] Bhattacharya AR, Maiti SN, Misra A, Morphology and Mechanical Properties of PA6/EVA Blends, J Appl Polym Sci, submitted for publication.
[27] Ide F, Hasegawa A. J Appl Polym Sci 1974;18:963.
[28] Joshi M, Misra A, Maiti SN. J Appl Polym Sci 1991;43:311.
[29] Chen HL, Wang SF. Polymer 2000;41:5157.
[30] Chen HL, Hsiao MS. Macromolecules 1998;31:6579.
[31] Liu LZ, Chu B, Penning JP, Manley RSJ. Macromolecules 1997;30:4398.
[32] Chen L, Li LJ, Lin TL. Macromolecules 1998;31:2255.